Significant Wave Height Measured by Coherent X-Band Radar

Ruben Carrasco, Jochen Horstmann, and Jörg Seemann

***Abstract*— Significant wave height is one of the most important parameters for characterizing ocean waves and essential for coastal protection, shipping, as well as off shore industry operations. Within this paper, a robust method is introduced for retrieving significant wave heights from Doppler speed measurements acquired with a coherent-on-receive marine radar. The Doppler velocity is caused by the surface scattering in the line of site of the radar. To a huge extent its periodic component is induced by the orbital motions associated with surface waves. The proposed methodology is based on linear wave theory, accounts for projection effects caused by the fixed antenna look direction, and was applied to a coherent-on-receive radar operating at X-band with vertical polarization in transmit and receive. To show the overall performance of the method, a data set consisting of approximately 100 days of radar measurements was analyzed and used to retrieve significant wave heights. Comparisons to wave measurements collected by a wave rider buoy resulted in a root-mean–square (rms) error of 0.21 m and a bias of 0 m without any calibration parameters needed. To further improve the accuracy of significant wave height, a calibration factor needs to be accounted for, which improves the rms error to 0.15 m with a negligible bias of −0.01 m.**

***Index Terms*— Doppler radar, marine radar, remote sensing, sea surface electromagnetic scattering, surface waves.**

I. Introduction

SIGNIFICANT wave height is one of the most important property characterizing the ocean surface and is therefore monitored by the offshore industry for their daily operation. Today there are several instruments available that allow to measure ocean surface waves. The most common devices are wave rider buoys, which allow to measure high-resolution frequency spectra of the sea surface elevation by analyzing the buoy's displacement within a time frame of typically 30 min. From the resulting wave spectrum, all the other spectral parameters of the wave field can be deduced. However, as buoys are single-point measuring devices, the time series only allow to estimate statistical moments of the directional distribution by additionally analyzing the time series of horizontal displacement. In contrast, ground-based marine radars not only provide observations of the sea state both in space and time, but also they can be easily deployed and have low maintenance costs. Nowadays marine radar image sequences are used operationally to retrieve various oceanographical and meteorological parameters [1]. Beside the 2-D wave spectra [2] and significant wave height [3], they also have shown to be useful to retrieve individual waves [4] and wave groups [5]. Furthermore, they can be used to retrieve near-surface currents [6], [7], bathymetry [8], as well as to monitor surface features [9]. Additionally, they have shown to be very useful for measuring wind speed and direction from platforms as well as from moving vessels [10].

However, in order to obtain reliable estimates of significant wave height from in coherent marine radars, with an accuracy of up to 0.3 m, an extensive calibration has to be performed to parameterize the modulation transfer function (MTF) relating radar backscatter intensity to significant wave heights [3], [11]. This is a challenging problem as the MTF is influenced by many factors, such as wind, waves, and currents, as well as the radar wavelength, polarization, incidence angle, and look direction. In addition, marine radars are not calibrated for the normalized radar cross section and therefore, the MTF has to be parameterized for every individual radar system and setup.

Utilizing coherent marine radar systems provides, in addition to intensity, the radial surface speed of the surface scatter elements. Although there are many different sources contributing to the radial speeds, the periodic modulation is primarily induced by the orbital motion of the ocean surface waves. Therefore, the radar-retrieved radial velocities have been used to measure significant wave heights. Hwang *et al.* [12] and Carrasco *et al.* [13] were able to obtain the significant wave height from the variation of the measured Doppler speed. Both used empirical approaches, with root-mean-square (rms) errors of, respectively, 0.32 and 0.24 m utilizing the same data set [13]. In this paper, a physics-based methodology for retrieving the significant wave height from radar-retrieved Doppler speeds is developed using the same data set as in the work of Carrasco *et al.* [13]. The main advantage of a physical approach is that it should be calibration free, and thus usable in any sea state conditions.

To obtain stable Doppler velocities, the radar has to observe the same points over a relatively long time period. This is achieved by pointing the radar antenna into the peak wave direction, which will only allow to measure the orbital velocity component in the radar look direction. Then, the directional wave spectrum is retrieved from the radar data acquired with rotating antenna [2]. The spectrum is used to detect the peak

Manuscript received January 20, 2017; revised March 15, 2017; accepted April 17, 2017. Date of publication July 17, 2017; date of current version August 25, 2017. This work was supported in part by the German Federal Ministry for Economic Affairs and Energy (BMWi) under Award 0327533C and Award 0325915C, and in part by the Coastal Observing System for Northern and Arctic Seas. *(Corresponding author: Jochen Horstmann.)*

The authors are with the Helmholtz-Zentrum Geesthacht Zentrum für Materialforschung und Küstenforschung, Department of Radar Hydrograhy, Institute of Coastal Research, D21502 Geesthacht, Germany (e-mail: jochen.horstmann@hzg.de).

Color versions of one or more of the figures in this paper are available online at http://ieeexplore.ieee.org.

Digital Object Identifier 10.1109/TGRS.2017.2706067

wave direction, and thus to estimate the loss of velocity due to the projection of the orbital velocity vector in the antenna look direction. In order to remove Doppler speeds that are not due to the waves, some filtering in the wavenumber–frequency domain is performed, which is based on the dispersion relation of linear surface waves. Finally, using linear wave theory, the velocity variance spectrum is transformed to a surface elevation spectrum from which the significant wave height is computed. Comparison with buoy measurements showed an overall good agreement with an rms error of 0.21 m, and with a negligible bias. However, the mean frequency from the radar-retrieved surface elevation spectrum deviates significantly from the *in situ* measurements. To overcome this deviation a tuning parameter was defined, matching the mean frequency between buoy and radar. This leads to an rms error of 0.15 m for significant wave heights.

The paper is organized as follows. Section I provides an overview over the oceanographic and hydrographic parameters that influence the backscatter intensity and Doppler velocity measured by the radar. In Section II, the utilized radar as well as experimental setup at the offshore research platform Fino-3 is described. The methodology for retrieving significant wave height from the coherent radar is presented in Section III. In Section IV, the methodology is validated by comparison of radar-retrieved significant wave heights to those of a buoy, using measurements collected over 3 months at the Fino-3 platform. In Section V, conclusions and perspectives for future work are presented.

A. Radar Sea Clutter

Marine radars operate in X-band at grazing incidence ($>85°$), where the backscatter of the ocean surface is primarily caused by the small-scale surface roughness, which is strongly dependent on the local wind [10]. For vertical polarization in transmit and receive (VV polarization), the main scattering mechanism is Bragg scattering, meaning that the radar backscatter is proportional to the spectral density of the surface roughness on scales comparable to half of the radar wavelength ($\sim$1.5 cm). In addition, especially for horizontal polarization in transmit and receive (HH polarization), radar backscatter is induced by other scattering mechanisms, e.g., wedge scattering or small-scale wave breaking. Long surface waves modulate the small-scale surface roughness that in turn modulates the radar backscatter. At grazing incidence, the main modulation mechanisms are tilt and hydrodynamic modulation, as well as shadowing of the radar beam due to the surface waves. At small grazing angles shadowing is the dominant modulation mechanism, even though at microwave frequencies, especially for VV polarization, diffraction in the geometrical shadow zone is observed [14]. Observations of radar backscatter at grazing incidence angle have shown that in the geometrical shadow zone, the backscatter intensity is strongly reduced and the signal-to-noise ratio (SNR) of the Doppler spectra is very low [15]. Therefore, in most studies, these areas are treated like geometrical shadowing. For a detailed description of scattering and modulation mechanisms at low grazing incidence, the reader is directed to a special issue on grazing incidence backscatter from rough surfaces [16].

Coherent radars allow to measure, in addition to the intensity, the Doppler speed of the backscattering elements. Various mechanisms have been observed at grazing incidence [17], [18], which contribute to the measured Doppler speed

$$u_D = u_{\mathrm{Br}} + u_{\mathrm{win}} + u_{\mathrm{cur}} + u_{\mathrm{orb}} + u_{\mathrm{bre}} + u_{\mathrm{inc}}. \tag{1}$$

Here u_{Br} is the speed of the Bragg scattering waves, u_{win} is the wind-induced surface drift due to wind shear stress at the air–sea boundary layer, and u_{cur} is the near-surface current velocity. The orbital speed of the waves u_{orb} contributes to the Doppler speed as a primary periodic modulation term. A possible minor periodic contribution could also be induced by the wind surface shear stress over the wave profile [19], [20]. The breaking of surface waves induces a further Doppler shift u_{bre}, which in magnitude is comparable to the phase speed of the waves during a breaking event (i.e., nonperiodic and of short duration). The contribution u_{inc} describes an additional Doppler shift, which appears at grazing incidence and is most likely due to the effect of shadowing of surface waves.

The backscatter intensity, modulation depth, and Doppler speed depend on the polarization of the radar antenna. For VV polarization, Bragg scattering is the dominant backscatter mechanism, whereas for HH polarization the backscatter is strongly due to micro breakers which are faster than the Bragg waves. Furthermore, for VV polarization there is more diffraction into the geometrical shadow zone at the troughs of the waves than at HH [14].

B. Linear Surface Waves

Following linear wave theory, the periodic contribution of the measured Doppler speed can be related to the orbital velocities of surface waves, which in turn are related to the wave height. Coherent measuring instruments such as the acoustic Doppler current profiler (ADCP) and the coherent marine radar enable to measure Doppler speeds close to (ADCP) or at the surface (coherent marine radar) and therefore wave height. This approach was used by Krogstad *et al.* [21] and later by Herbers *et al.* [22] to measure high-resolution directional wave spectra of surface gravity waves with an up-looking ADCP. Comparison of their ADCP measurements to those obtained by pressure sensors resulted in errors less than 10%. Today this technique is used operationally to obtain wave information from ADCPs.

Measuring the horizontal component of the orbital velocity in the radial direction ϕ_r is necessary to estimate the transfer function between the radial velocity spectrum S_{v_r} and the surface elevation spectrum S_ξ, as given by

$$S_{v_r}(k_x, k_y, \omega) = K^2\sigma^2 \cos^2(\phi(k_x, k_y) - \phi_r) S_\xi(k_x, k_y, \omega) \tag{2}$$

where σ is the intrinsic frequency, ω is the absolute frequency, ϕ is the wave direction, and the depth dependence factor is

$$K = \frac{\cosh(kz)}{\sinh(kd)}. \tag{3}$$

$$r_P = \frac{m_{0,P}}{m_0} = \frac{\int \cos^2(\phi(k_x,k_y)-\phi_r) S_\xi(k_x,k_y,\omega) F_D(\omega-\Omega(k_x,k_y)+\vec{k}\vec{u}) dk_x dk_y d\omega}{\int S_\xi(k_x,k_y,\omega) F_D(\omega-\Omega(k_x,k_y)+\vec{k}\vec{u}) dk_x dk_y d\omega} \tag{7}$$

Here k is the wavenumber which is connected with the intrinsic frequency by the linear dispersion relation $\Omega\ (k)$

$$\sigma = \Omega(k) = \sqrt{gk\tanh(kd)} \tag{4}$$

where d is the water depth and z is the distance of the sensor to the bottom. In the case of the radar, the orbital velocity is measured at the sea surface, so z is equal to d (approximating the vertical position on the wave profile with the mean water level). The absolute frequency of the waves ω as measured in the frame of reference of the radar and the intrinsic frequency σ as observed in a frame of reference moving with the near-surface current are connected by

$$\sigma = \omega - \vec{k}\vec{u} = \omega - (k_\parallel u_\parallel + k_\perp u_\perp) \tag{5}$$

where $\parallel$ and $\perp$ are, respectively, the parallel and perpendicular components of the projection direction ϕ_r. The term $\cos^2(\phi-\phi_r)$ describes the projection of the orbital velocity vector in the direction ϕ_r for each spectral component of the wave field. For deep water ($kd > 0.25$), the depth dependence factor and the linear dispersion relation simplify to $K = 1$ and $\sigma = \Omega(k) = \sqrt{gk}$.

This kind of a setup was used by de Schipper *et al.* [23] to measure the shoaling transformation of surface waves with a horizontally looking ADCP and it is identical to the setup of the coherent marine radar at grazing incidence.

C. Radial Projection

For the retrieval of significant wave height from radar measured radial Doppler velocities, Carrasco *et al.* [13] followed a purely empirical approach, while Hwang *et al.* [12] used a method based on linear wave theory. However, neither took into account the loss of spectral power due to the projection of the orbital velocity vector in the antenna viewing direction. This power loss is unavoidable due to the directionality of natural sea states and is especially large for a multimodal sea. Rearrangement of (2) results in a description of the spectral power loss due to the projection of the orbital velocity vector (projected heave spectrum)

$$\begin{aligned} S_{\xi,P}(k_x,k_y,\omega) &= \cos^2(\phi\ (k_x,k_y)-\phi_r) S_\xi(k_x,k_y,\omega) \\ &= \frac{S_{v_r}(k_x,k_y,\omega)}{K^2\sigma^2}. \end{aligned} \tag{6}$$

The right-hand side describes the velocity to heave transform according to linear wave theory. The left-hand side makes clear that the retrieved heave spectrum is already affected by the spectral power loss due to the projection of the orbital velocity vector. Therefore, a "projection loss" ratio r_p can be defined as (7), as shown at the top of the page, where $m_{0,P}$ is the spectrum of the surface elevation, projected in the radar look direction, and m_0 is the total spectral energy. Here F_D is a spectral mask that excludes the portion of the spectrum that does not follow the wave dispersion relation (4). The projection loss ratio r_p gives the relative loss of total spectral energy due to projection. It can be estimated from the 3-D wavenumber–frequency spectrum of a radar image sequence, acquired with rotation mode (Section II).

Within this study, the Doppler speed measurements are acquired with the radar pointing into the peak wave direction (Section II). Therefore, the observation of the waves in the 2-D range-time domain results in a projection of the 2-D wavenumber vector in the antenna look direction, $k_\parallel = k(\cos\phi - \rho_r)$. In the 2-D case, the transformation of the orbital velocity spectrum to a surface elevation spectrum is described by

$$S_{\xi,P}(k_\parallel,\omega) = \frac{S_{v_r}(k_\parallel,\omega)}{K^2\sigma^2} \tag{8}$$

instead of (6). The depth dependence factor K depends on the product kd. To estimate the significant wave height from the total energy of the 2-D wavenumber–frequency spectrum, the energy has to be corrected for the projection loss ratio. In (7), the projection loss ratio is defined for the general case that the wave field is observed in the 3-D space-time domain (x, y, t). The 2-D wavenumber surface elevation spectrum is deduced from a radar image sequence [2], [3], and the projection loss ratio is then obtained from

$$r_P = \frac{m_{0,P}}{m_0} = \frac{\int \cos^2(\phi(k_x,k_y)-\phi_r) S_\xi(k_x,k_y) dk_x dk_y}{\int S(k_x,k_y) dk_x dk_y}. \tag{9}$$

For this study, a directional wave rider buoy is used for validation purposes. One parameter to be validated is the projection loss ratio. The buoy measures the directionality of the wave field in the directional frequency domain, and the projection loss ratio estimated from the buoy data is expressed as

$$r_{P,\text{buoy}} = \frac{\int \cos^2(\phi-\phi_r) S(\omega,\phi) d\omega d\phi}{\int S(\omega,\phi) d\omega d\phi}. \tag{10}$$

II. Experimental Setup

All data used for this study were collected at the offshore research platform Fino-3, which is located 80-km west of the island of Sylt, within the German Bight in the southern North Sea [Fig. 1(a)]. The water depth at the platform's location is 22 m, and depths slightly increase to 27 m within 3 km to the Northwest of the platform. Fino-3 is equipped with a large number of meteorological and oceanographic measurement devices, which provided sea state, current and surface wind data for this study. The radar data recorded at Fino-3 were acquired by a 12-kW marine radar, operating at X-band (9.3 GHz) with vertical polarization in transmit and receive (VV-pol) at a height of 43 m. To retrieve Doppler information the system was operated as a coherent-on-receive radar system [24], which means that the random and uncorrelated phases of the radar pulses were recorded and taken

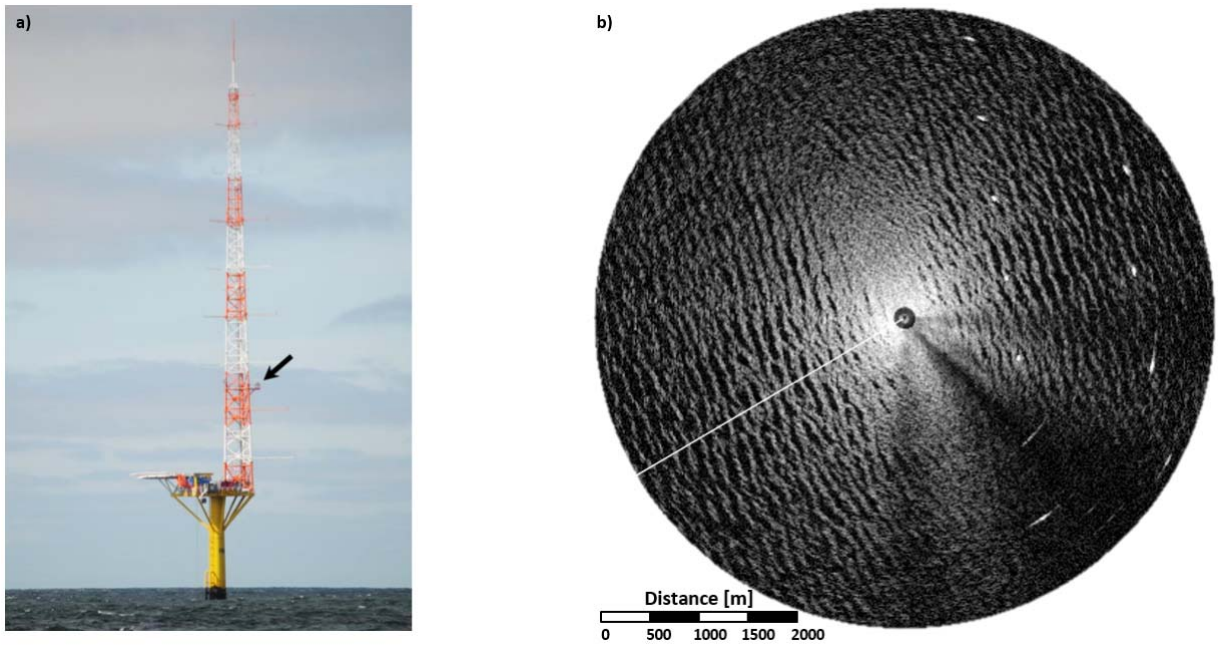

Fig. 1. (a) Research platform Fino-3 located in the German Bight hosting the marine radar (small arrow). (b) Marine radar intensity image acquired in the rotational mode at Fino-3. The white line depicts the radar-retrieved peak wave direction, which is used to orientate the radar antenna for the static mode.

into account within the post processing to retrieve the complex backscattered signal from the sea surface. The pulse repetition frequency of the radar was set to 1 kHz, which allowed to measure a maximum radial Doppler speed of ± 8 m/s without aliasing. The radar was operated with a pulselength of 50 ns, which resulted in a range resolution of 7.5 m. The antenna had a vertical beam opening of 21° and a width of 7.5 feet (2.3 m) resulting in an azimuthal resolution of $\sim 1°$. The radar signal was run through a linear amplifier and then digitized with 13 b up to a range distance of 3262.5 m. Within this study, the radar was operated in two different modes, the rotation and static modes. In the rotation mode, the radar acquired 360° azimuthal scans of the ocean surface at a rotation speed of 1 rad/s, which resulted in radar images covering the entire range [Fig. 1(b)]. In the static mode, the radar antenna was oriented in a user selected fixed direction [white line in Fig. 1(b)] and acquired data for a predefined amount of time over range. The data used within this study were acquired between March 6 and July 14, 2015 and covered a large range of wind speeds (1–23 m/s) and significant wave heights (0.2–4.9 m). Within this time period, the radar was scheduled with an hourly cycle starting with 10 min of rotational data, which were utilized to retrieve the wave spectra and in particular the peak wave direction [3]. Within the following 32 min, ten predefined directional scans were acquired in the static mode, which were not used within this study. After these ten acquisitions the antenna was oriented into the radar-retrieved peak wave direction (looking up-wave) to acquire 15 min of data in the static mode. From the collected 2653 hourly cycles, 90 cycles have been removed. In 87 of these cases the radar signal was too weak and three cases were removed due to very heavy rain.

In addition to the radar data, the 10-min mean wind speed and wind direction measurements recorded at Fino-3 at a height of 30 m were used. The wind speed and direction measurements were obtained by a cup anemometer and a wind vein, respectively. For calibration as well as validation purposes, wave measurements were recorded by a Mark III directional wave rider buoy, moored within the vicinity ($<$200 m) of the Fino-3 platform. The buoy measured its orbital path with a sampling rate of 1.28 Hz. These data provided the standard spectral sea sate parameters such as the significant wave height, peak wave direction, peak wave period, and directional wave spectra as well as the individual wave heights. Finally, a bottom mounted acoustic wave and current profiler (AWAC) acquired current profiles in 13 water depths, the water level, as well as wave spectral information in the vicinity ($<$100 m) of Fino-3.

III. Data Processing

All The radar data acquired in the rotational mode were used to retrieve the peak wave direction, which was needed to determine the orientation of the radar antenna for acquisition in the static mode. To estimate the peak wave direction, the well-known method based on filtering with the dispersion relation was used [3]. Therefore, the radar image sequence was converted from the spatial temporal domain into the wavenumber–frequency domain via a 3-D fast Fourier transform (FFT). In the wavenumber–frequency domain, the wave energy is located on a shell, which is defined by the linear dispersion relation of surface waves (4). This dispersion shell was used as a filter to collect the wave energy, which resulted in a significant noise reduction in the power spectra. In the final step, the MTF from the image power spectrum to a wave power spectrum was applied [3]. Note that the wave power spectrum is not calibrated!

To estimate the significant wave height from the coherent marine radar data, several processing steps need to be

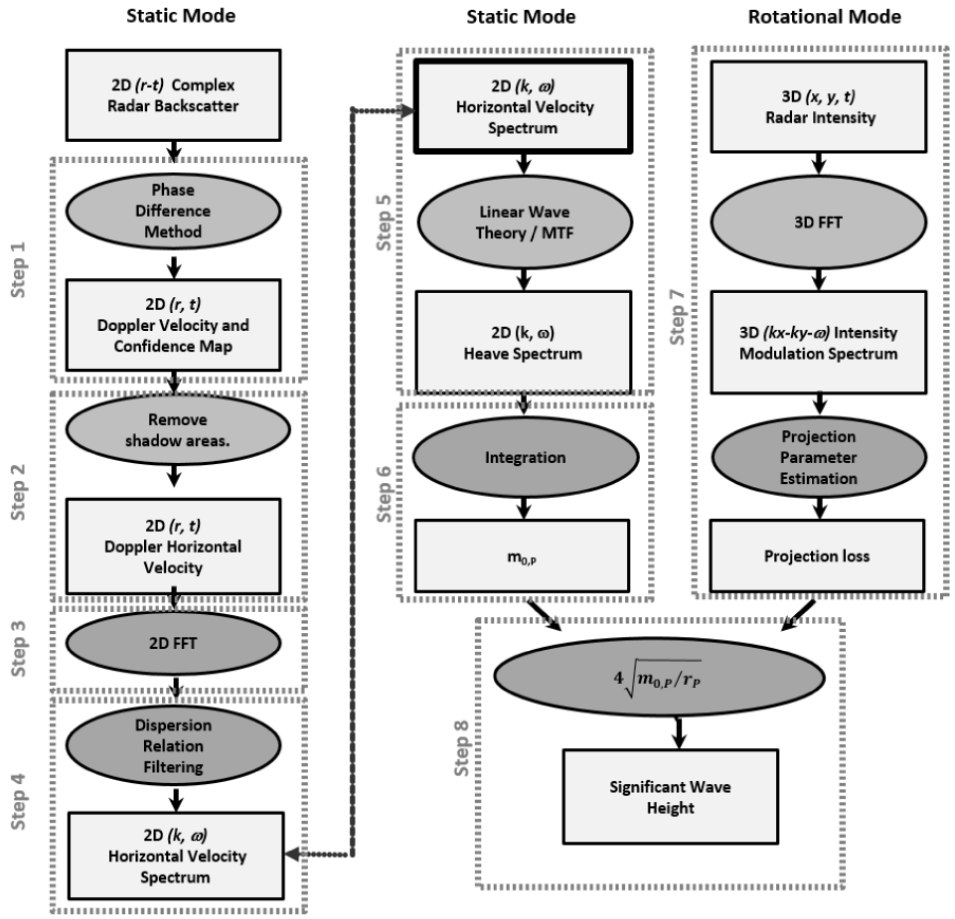

Fig. 2. Schematic showing the processing steps to retrieve significant wave height from coherent marine radar data.

followed, which are summarized in the schematic shown in Fig. 2. Steps 1–6 describe the processing of the data acquired in the static mode with the radar pointing into the peak wave direction. In contrast to Hwang *et al.* [12], who collected data only over a few seconds (5 and 15 s), the data here were collected over a period of 15 min to ensure a larger statistical sample of waves comparable to that used in wave buoy measurements (typically 30 min). Within step 7 the projection loss ratio, introduced in (9) of Section I-C, is estimated from the radar data acquired in the rotational mode. The individual steps are described as follows.

Step 1 (Doppler Speed and Confidence Retrieval): The Doppler speeds were retrieved from the radar data acquired in the static mode by applying the so-called "pulse-pair method" [25]. Therefore, the Doppler shift frequency f_D was computed using the derivative of the instantaneous phase ϕ_{el} of the coherent radar signal

$$f_D = \frac{1}{2\pi}\frac{d\phi_{\mathrm{el}}}{dt} = \frac{1}{2\pi} d\phi_{\mathrm{el}} \mathrm{PRF}. \tag{11}$$

Here, t is time and PRF is the pulse repetition frequency of the radar. The corresponding horizontal Doppler speeds were obtained from

$$u_D = \frac{\lambda_{\mathrm{el}}}{2\cos(\gamma)} f_D \tag{12}$$

where λ_{el} is the electromagnetic wavelength of the radar and γ the grazing angle, which is needed to compute the horizontal contribution of the Doppler speed. To reduce the noise of the calculated Doppler speeds, the frequency shifts of a chunk of 512 pulses were averaged.

A confidence measure is given by the alignment of the vectors pointing to the phase difference in the complex plane

$$\mathrm{Conf} = \frac{|\sum C_j|}{\sum |C_j|}, \quad C_j = A_{j+1} e^{i(\Phi_{j+1} - \Phi_j)}. \tag{13}$$

Fig. 3(a) shows a plot in time and range of the mean Doppler velocities (step 1) resulting from the radar measurements recorded at Fino-3 on March 31, 2015 at 13:44 UTC. In Section I, the different contributions to the Doppler speed (1) are listed. The periodic variations of the Doppler speed are mostly due to the orbital motion of the waves in look direction; this is clearly shown in Fig. 3(a). In addition, an increase of Doppler speed with range can be seen in Fig. 3(a). This is most likely due to the effect of shadowing, which increases with range.

Step 2 (Identification of Shadowing): If the troughs of the wave profile are shadowed, only the electromagnetic field diffracted at the wave crests can reach the trough. Therefore, Doppler spectra from these parts of the sea surface have a low signal-to-noise ratio and with the radar utilized in this study,

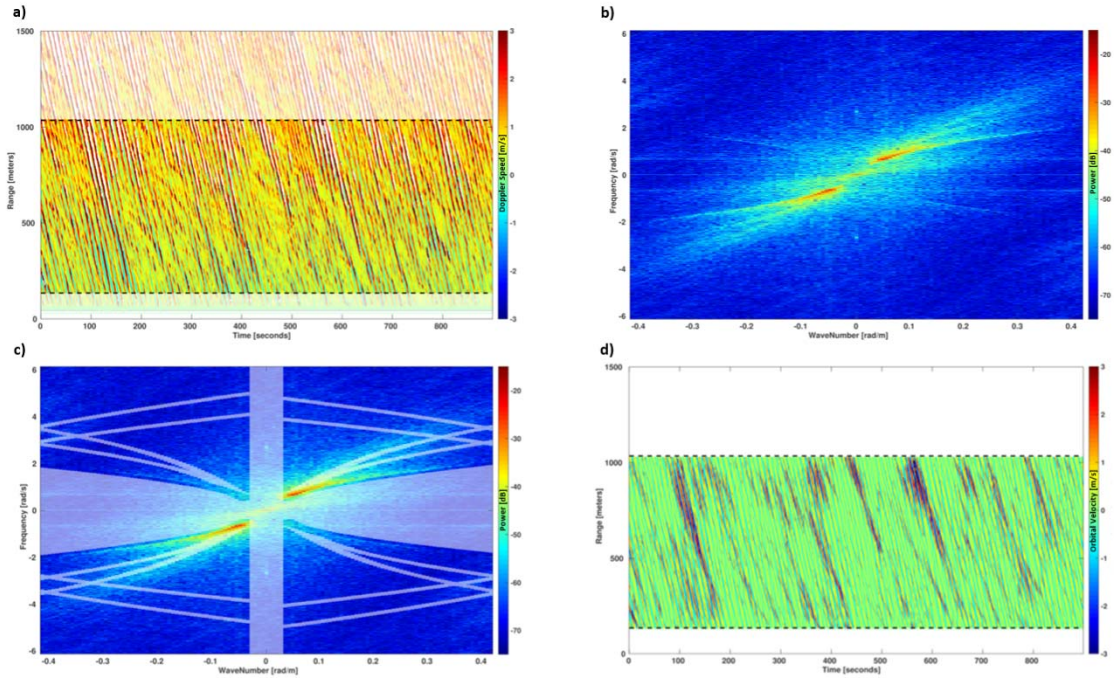

Fig. 3. (a) Plot of mean Doppler velocities (color coded) in time (x-axis) and range (y-axis) retrieved from the radar data acquired at Fino-3 on March 31, 2015 at 13:44 UTC. All Doppler speeds with a confidence level $\leq$0.6 are masked in soft white. (b) Doppler-velocity wavenumber–frequency spectra retrieved from (a). (c) Doppler-velocity wavenumber–frequency spectra retrieved from (a), where the part of the spectrum excluded for the significant wave height retrieval is masked in soft white. (d) Plot of mean Doppler velocities (color coded) in time (x-axis) and range (y-axis) retrieved from the radar data acquired at Fino-3 on March 31, 2015 at 13:44 UTC. All Doppler speeds with a confidence level $\leq$0.6 are masked in soft white, after application of the dispersion filter.

a reliable retrieval of Doppler velocities was not possible. As a low SNR results in a low confidence of the phase difference method, chunks with a confidence less than 0.6 (13) were considered as affected by electromagnetic shadowing [soft white shading in Fig. 3(a)].

Step 3 (Calculation of Doppler-Velocity Wavenumber–Frequency Spectra): For the retrieval of the Doppler-velocity spectra, the entire 15-min time record was used. However, a maximum range limit was set, where less than 10% of the data where marked as shadowed. The selected spatial–temporal measurements were transformed via an FFT into the wavenumber–frequency domain [Fig. 3(b)].

Step 4 (Filtering With the Dispersion Relation): Until recently, the dispersion relation of surface waves has been used as a spectral filter in the 3-D wavenumber–frequency spectrum [6], [7]. Here, this technique was applied to the 2-D projected wavenumber–frequency spectrum of the Doppler-velocity modulation. Due to the projection of the wave pattern, the dispersion relation defines a line in the wavenumber–frequency domain. This line can be understood as an upper bound for the wavenumbers at each frequency, because the projected wavenumber is smaller than the actual wavenumber. The resulting filter is shown in Fig. 3(c). Note that the dispersion relation is dependent on the current, so as a previous step, a current fit should be performed [6], [7]. It should be noted that the first and second harmonics from the dispersion relation were also removed [soft white shading in Fig. 3(c)].

Finally, the dispersion filter was applied by removing the spectral energy outside the filter domain. The dispersion filter removes all nonperiodic contributions to the Doppler velocity, such as those from the surface current, the wind, and the range-dependent Doppler shift. This can be seen in Fig. 3(d), which shows the Doppler velocities after an inverse 2-D FFT of the filtered spectrum was applied to Fig. 3(c).

Step 5 (Transformation From Velocity to Heave): The transformation from the power spectra of horizontal orbital velocities to the surface elevation power spectra was performed by applying linear wave theory (3). In Section IV, it is shown that the retrieval can be improved by replacing the factor $1/\omega^2$ by $1/\omega^\beta$ in (8), with $\beta = 1$. The physical reason for this particular value of β is unknown, and this new factor constitutes an empirical MTF.

Step 6 (Integration of Spectral Power): By integration over the wavenumber coordinate, a 1-D frequency spectrum was calculated. This frequency spectrum is not yet a true surface elevation spectrum, because each frequency bin is affected by the projection loss ratio, which depends on the directionality at that frequency and the antenna look direction. Here it is termed a projected surface elevation spectrum and is used for validation purposes in Section IV. By integration over the wavenumber and frequency coordinates, the total variance $m_{0,P}$ of the projected surface elevation spectrum was obtained. This magnitude was used to estimate the significant wave height.

Step 7 (Estimation of Projection Loss Ratio): The projection loss ratio r_p was estimated from the 2-D wavenumber spectrum (9), computed from the radar image sequence acquired in the rotation mode. Here the intensity spectrum was used instead of the surface elevation variance spectrum, as the method is more robust. The transfer function between intensity

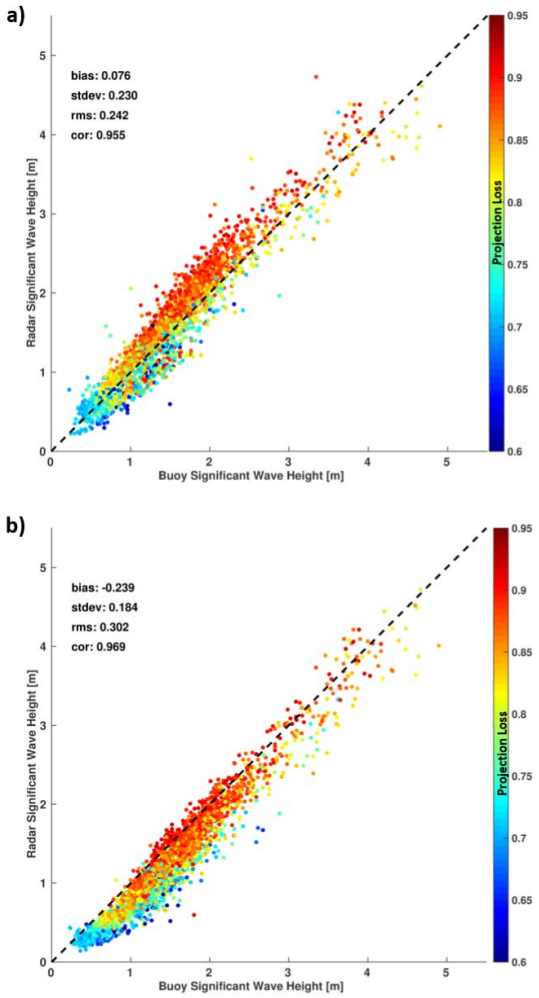

Fig. 4. Scatter plot of significant wave heights resulting from the buoy at Fino-3 and simple empiric radar approach (a) from Carrasco *et al.* [13] and (b) from the radar approach introduced in Section III utilizing linear wave theory in step 5 and excluding step 7. The color coding represents the projection loss ratio (9).

and surface elevation spectrum depends on the shape of the wave spectrum (wind sea versus swell). Comparing the projection loss ratio estimated from intensity and surface elevation spectrum only shows only a minor influence on the retrieval of significant wave height.

Step 8 (Significant Wave Height Retrieval): The significant wave height was computed from

$$H_S = 4\sqrt{\frac{m_{0,P}}{r_p}}. \tag{14}$$

IV. Validation and Discussion

For the validation of the different steps within the retrieval of significant wave height, the buoy data collected in the vicinity of Fino-3 were compared to the results obtained from the radar. Fig. 4(a) shows the scatter plot of the simple empirical approach followed by Carrasco *et al.* [13] and Fig. 4(b) from the methodology explained above utilizing linear wave theory in step 5 and neglecting step 7 (the projection loss ratio). Although the later method has a significantly lower standard deviation, it results in a significant bias of −0.24 m. As the radar only measures the orbital velocity

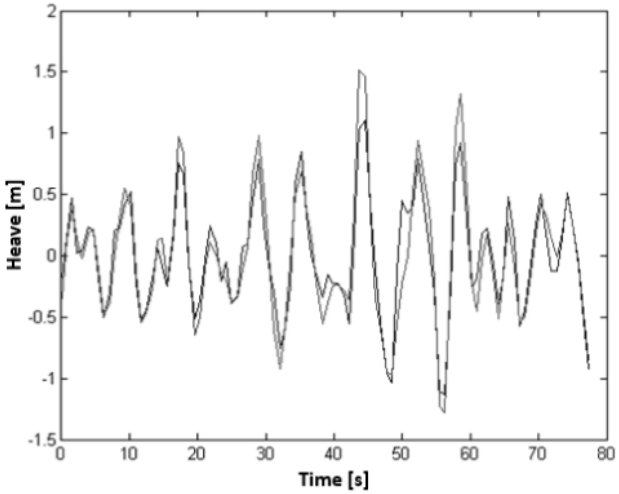

Fig. 5. Plot shows heave resulting from the horizontal displacement of the buoy (gray line) and computed from the horizontal orbital velocity following linear wave theory and applying the projection loss ratio (black line).

in the look direction of the radar, the contribution of the orbital velocity of waves not traveling in line of sight of the radar lead to an underestimation of the orbital velocity and therefore of the significant wave height. Note that within the empirical approach no dispersion relation filtering has been performed (step 4) and therefore all the measured variance is considered for the retrieval of significant wave height. In step 7, the projection loss ratio has been estimated under consideration of the directional wave spectrum retrieved from the radar. In general, the color coding in Fig. 4 gives the projection loss ratio. In Fig. 4(b), it can be seen that the projection loss ratio decreases with increasing differences between buoy and radar-retrieved significant wave height.

The directional wave rider buoy used within this study measures the vertical and horizontal movement induced by the waves. Therefore, the methodology for retrieving significant wave height from the radar-retrieved horizontal orbital velocity was tested using the buoy raw data (excluding the spectral filtering). From the vertical displacement time series the significant wave height was deduced using $H_s = \mathrm{std}(z(t))$, which is in agreement with the spectral estimation $H_s = 4\sqrt{m_0}$. From the horizontal displacement, the horizontal orbital velocity vector was calculated. To simulate the radar data processing workflow the peak wave direction was estimated from the directional wave spectrum of the buoy and the orbital velocity vector was projected in the peak wave direction, creating a radial velocity time series. From this point on, steps 5 (using linear wave theory) through 8 were followed to calculate the significant wave height. In Fig. 5, the heave is shown for an 80-s time series resulting directly from the heave measured by the buoy (pink line) and resulting from the buoy's horizontal orbital velocity (blue line) following the methodology described above. It can be seen that both methods agree very well with each other.

To validate the significant wave height retrieval methodology from Doppler radar the 3-D orbital path recordings from the directional waverider buoy at Fino-3 were used. From

the buoy data the directional wave spectrum and significant wave height were estimated. To validate the Doppler radar processing scheme the significant wave height was retrieved from the buoy by projecting the orbital velocity vector in the antenna viewing direction and then following steps 5 through 8 of Section III. Fig. 6(a) depicts the scatterplots of significant wave heights retrieved from the buoy heave versus the values estimated from the reconstructed surface elevation spectrum (radar method) excluding the correction for projection loos. As expected the significant wave height is underestimated due to the projection loss effect (bias = 0.16 m). In Fig. 6(b), the same scatter plot is shown, however, after correcting the total spectral energy of the reconstructed surface elevation spectrum with the power loss ratio. Now, unexpectedly the significant wave height is overestimated (bias = 0.14 m). This bias is observed for both low and high sea states. A possible reason for this could be the directional spreading of the wave field, which may be overestimated by the buoy. To test this hypothesis the projection loss ratio was also estimated from the radar intensity images, which are superior to the buoy with respect to the resolution of the directionality of the wave field. However, there is still an overestimation of the significant wave height (bias = 0.09 m). In the future work this bias will have to be investigated in more detail.

The limited spatial resolution of the radar implies a frequency cutoff of the retrieved surface elevation spectrum, which leads to a missing high-frequency tail and therefore an underestimation of the significant wave height. This effect was also investigated with the buoy data. Therefore a cutoff wavelength of 15 m was assumed that corresponds, according to linear wave theory, to a cutoff frequency of 2.03 rad/s, which resulted in a bias of −0.07 m for significant wave height. For a radar with a cutoff wavelength of 30 m, corresponding to a frequency of 1.43 rad/s the bias increases to −0.22 m. Due to the integration of the complex backscatter over the radar pulselength the modulation spectrum is low-pass filtered over the wavenumber domain. For the radar used here, the attenuation starts at a wavelength of 30 m and waves with a wavelength of 15 m are totally lost. In summary, the comparison with buoy data shows that the overestimation of significant wave heights due to consideration of the projection loss ratio and the underestimation due to the loss of energy in the high-frequency tail of the wave spectrum partially compensate each other. However, the exact value of a possible bias depends on the setting of the radar pulselength.

Validation of the radar-retrieved significant wave height resulting from steps 1 through 8 under consideration of linear wave theory in step 5 resulted in the scatter plot shown in Fig. 7. When the projection loss ratio was retrieved from the buoy data the rms error decreased to 0.22 m with a negligible bias of 0.01 m and applying the radar-retrieved projection loss ratio resulted in an rms error of 0.21 m with a bias of 0 m. As there is almost no difference between the two values, the projection loss ratio obtained from the radar data was considered robust enough to be used.

When comparing the mean frequencies of the radar heave spectra with those of the projected buoy heave spectra, a standard deviation of 0.3 rad/s was found, with a significant bias of −0.25 rad/s. To compensate for this frequency shift, the horizontal velocity to heave transfer function according to linear wave theory in step 5 is replaced by an empirical MTF

$$H(\omega) = \omega^{-\beta} \tag{15}$$

where β is an empirical calibration constant. In Fig. 8(a), the calibration constant β is plotted versus the rms error, standard deviation, and bias resulting from the comparison of the mean frequency from the buoy spectrum and that of the radar spectrum. It can be seen that setting $\beta = 1$ results in a mean frequency bias of 0 as well as in a very small rms error. Similar results are shown in Fig. 8(b) where the calibration constant β is plotted versus the error in significant wave height. Also, in this case the lowest rms error is observed for a β of approximately 1. In Fig. 9, the comparison of significant wave heights resulting from the buoy measurements to those from the radar is shown, here the radar-retrieved significant wave heights were computed utilizing steps 1 through 8 under consideration of the empirical MTF in step 5 with $\beta = 1$. The

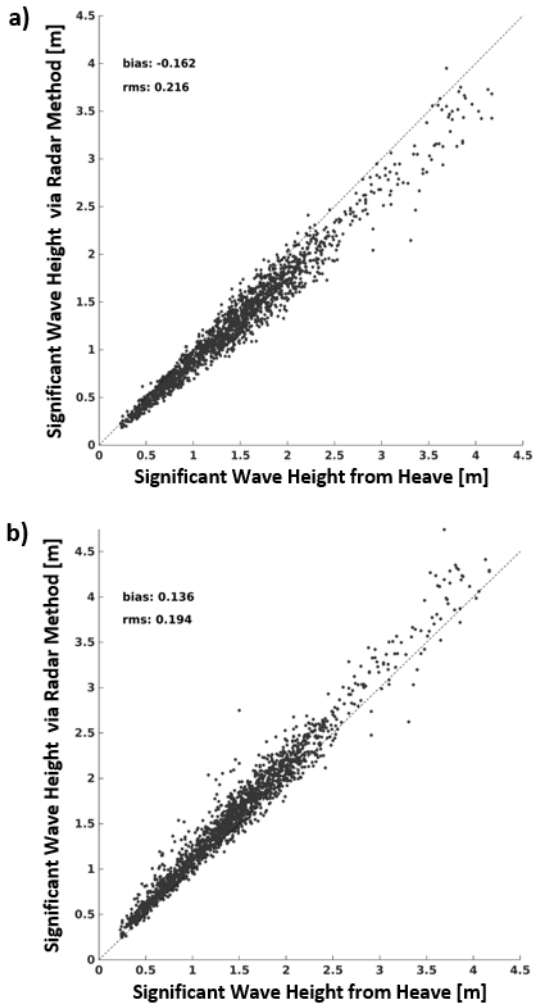

Fig. 6. Scatterplot of significant wave height resulting from the heave measurements of the buoy versus those retrieved from the reconstructed surface elevation spectrum (a) excluding and (b) including the projection loss ratio.

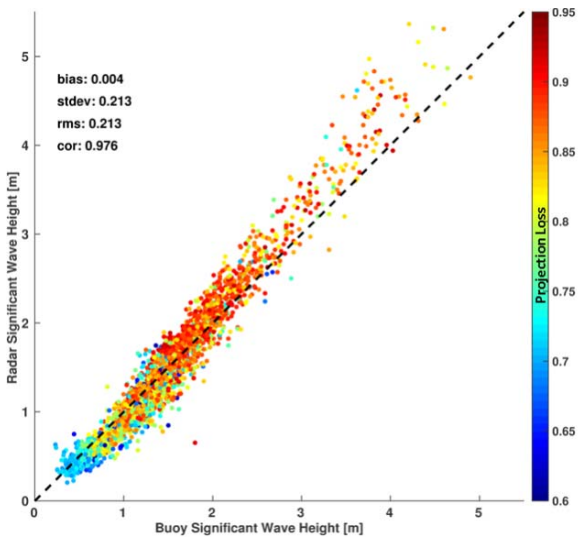

Fig. 7. Scatter plot of significant wave heights resulting from the buoy at Fino-3 and the method introduced in Section III using linear wave theory in step 5 and including the projection loss ratio in step 7. The color coding represents the projection loss ratio (9).

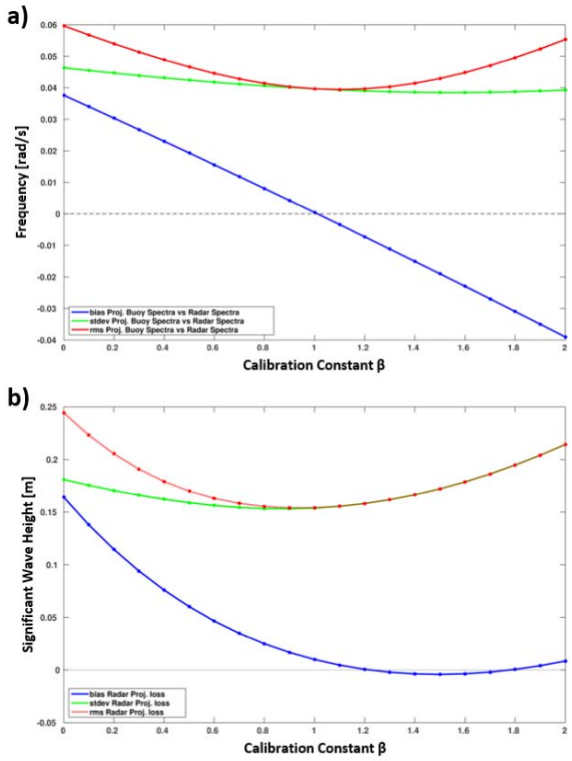

Fig. 8. (a) Bias, standard deviation, and rms error of mean wave frequencies resulting from the comparison of the buoy spectrum to the radar spectrum at different values of the calibration constant β. (b) Bias, standard deviation, and rms error of the significant wave height resulting from the comparison of the buoy to the radar at different values of the calibration constant β.

comparison results in a correlation of 0.98 with an rms error of 0.15 m and a negligible bias of 0.01 m.

When estimating significant wave height from backscatter intensity image sequences, one of the major sources of error is due to the differences occurring at wind and swell-dominated seas. Typically the significant wave height is underestimated

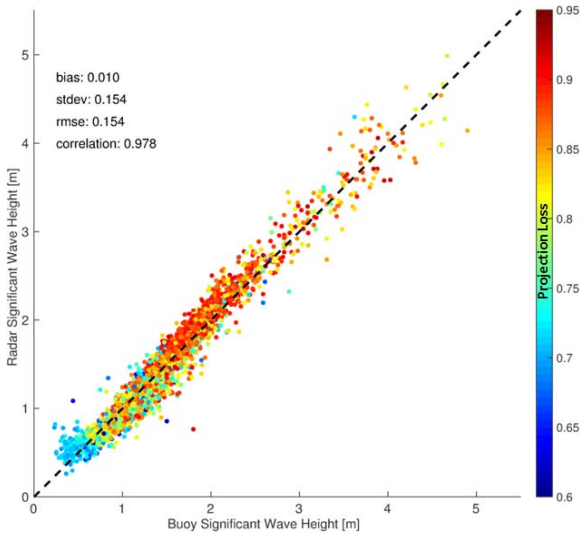

Fig. 9. Scatter plot of significant wave heights from the buoy and the Doppler radar utilizing step 1 through 8 and the empiric MTF with $\beta = 1$ in step 5. The color coding represents the projection loss ratio (9).

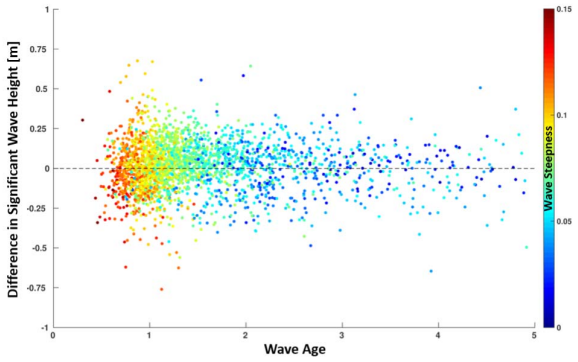

Fig. 10. Dependence of the differences in radar-retrieved significant wave height on wave age. The color coding represents the wave steepness.

under swell-dominated seas [11]. Therefore, here the sea state was characterized by the wave age, which is defined as the ratio of the phase speed of the dominant waves to the wind speed at a reference height of 10 m. A wave age of 1.2 refers to fully developed seas, while smaller values indicate young seas, and large values swell. In Fig. 10, the wave age is plotted versus the difference between buoy and radar-retrieved significant wave heights. The color coding refers to ε the steepness of the waves, which is defined as

$$\varepsilon = k_p \frac{H_S}{2} \tag{16}$$

where k_p is the wavenumber at the peak wave period. It can be seen that the scatter is larger at young seas but that there is no trend (bias) with respect to wave age. Also with regards to steepness of the waves there is no trend within the differences of significant wave height within the comparison data set. Note that for significant wave height retrieval via the SNR ratio both the wave age as well as wave steepness lead to a significant bias [11].

To get a better indication on the accuracy of the significant wave retrieval from the radar, a comparison to results from

TABLE I

MAIN STATISTICAL PROPERTIES RESULTING FROM THE COMPARISONS OF SIGNIFICANT WAVE HEIGHTS RESULTING FROM DIFFERENT SOURCES, E.G., BUOY, AWAC, AND RADAR WITH (WT) AND WITHOUT TUNING (NT) BY β

	Buoy to AWAC	Buoy to Radar WT	Buoy to Radar NT	AWAC to Radar WT	AWAC to Radar NT
Bias	0.01 m	-0.01 m	0.00 m	-0.02 m	-0.03 m
Stdev	0.09 m	0.15 m	0.21 m	0.15 m	0.24 m
Rmse	0.09 m	0.15 m	0.21 m	0.16 m	0.24 m
Cor	0.99	0.98	0.98	0.98	0.97 m

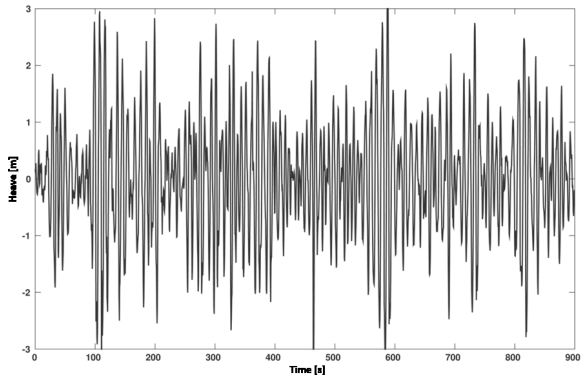

Fig. 11. Time record of heave resulting from Doppler speeds measured at a distance of 800 m to the radar. The data were acquired at Fino-3 on March 31, 2015 at 13:44 UTC (see Fig. 3).

the wave rider and the (AWAC) was performed. The statistical properties of the comparison are summarized in Table I. It can be seen that comparison between the buoy and AWAC are only slightly better than the comparisons of the radar results to the buoy and AWAC. This indicates the overall good performance of the radar-retrieved significant wave heights.

V. CONCLUSION

A methodology has been developed, tested and validated to retrieve the significant wave height from Doppler speed measurements acquired by a coherent-on-receive marine radar operating at X-band with vertical polarization in transmit and receive. In contrast to the pure empirical approach of Carrasco *et al.* [13] or the semi physical approach from Hwang *et al.* [12] that requires some calibration coefficients the method presented in this paper is based on physics and requires no calibration. Therefore, the radar acquires Doppler speed measurements from the ocean surface along the peak wave direction. These Doppler speeds are filtered utilizing the linear dispersion relation of surface waves, which enable to remove Doppler speed contribution not due to the waves, such as surface winds and currents. Assuming that the remaining Doppler speeds are equivalent to the horizontal orbital velocities induced by the waves, linear wave theory is applied to retrieve the significant wave height. The resulting significant wave heights are significantly underestimated due to the projection of the orbital velocity vector in the antenna viewing direction, which leads to a loss of spectral power induced by the multi directionality of sea state. The projection loss ratio is estimated from the 2-D wavenumber spectrum, which is retrieved from the radar image sequence acquired in the rotational mode following the well-known methodologies [2], [3]. Considering the projection loss ratio the significant wave heights can be retrieved from the Doppler speed measurements of the radar without need of any calibration. For validation purposes the radar-retrieved significant wave heights were compared to buoy measurements resulting in a correlation of 0.98 and an rms error of 0.21 m with a negligible bias (below 0.01 m). This accuracy is comparable to the best results obtained from intensity images were for every individual radar setup an intensive calibration has to be performed [26].

However, comparison of the mean frequencies of the projection loss ratio corrected radar heave spectra to the projected heave spectra of the buoy results in a standard deviation of 0.3 rad/s with a significant bias of -0.25 rad/s. To accommodate for this the factor $\sigma 1/^2$ in the transformation of the orbital velocity spectrum to a surface elevation spectrum is replaced by $\sigma 1/^\beta$, with $\beta = 1$, which is sort of an empirical MTF. Unfortunately, so far no experience has been gathered on the dependencies of the β and how it may change from setup to setup. Nevertheless, comparison of radar-retrieved significant wave heights (including the β) to the buoy results showed a correlation of 0.98 with an rms error of 0.15 m with a bias of 0.01 m.

Future investigations will concentrate on a getting a more detailed understanding on the physics contributing to the measured Doppler speeds. In particular to fully understand the mechanisms which have led to the mean frequency bias, which so far has been accounted for by the β correction. This will also help to understand how and how well the radar-retrieved orbital velocities [Fig. 3(d)] can be utilized to obtain an individual wave field, as shown in Fig. 11. This time record of wave heights was retrieved via linear wave theory from the orbital velocities obtained from the radar at a range of 800 m (Fig. 3). Furthermore, the effect of shadowing on the significant wave height retrieval will be investigated, which is particularly important as it will allow pushing the working range distance of the radar further out, which is in particular important for coastal stations. Last but not least it will also be of great interest to investigate the possibilities for retrieval of wave parameters utilizing HH polarization. In particular as initial observations of Doppler speed measurements at grazing incidence for VV- and HH-polarization show significant differences.

ACKNOWLEDGMENT

The authors would like to thank the Federal Maritime and Hydrographic Agency (BSH) for provision of the buoy and AWAC data at Fino-3.

REFERENCES

[1] J. Horstmann, J. C. N. Borge, J. Seemann, R. Carrasco, and B. Lund, "Wind, wave and current retrieval utilizing X-band marine radars," in *Coastal Ocean Observing Systems*. Amsterdam, The Netherlands: Elsevier, 2015, pp. 281–304, ch. 16.

[2] I. Young, W. Rosenthal, and F. Ziemer, "A three-dimensional analysis of marine radar images for the determination of ocean wave directionality and surface currents," *J. Geophys. Res.*, vol. 90, no. C1, pp. 1049–1059, 1985.

[3] J. C. Nieto-Borge, K. Reichert, and J. Dittmer, "Use of nautical radar as a wave monitoring instrument," *Coastal Eng.*, vols. 3–4, no. 37, pp. 331–342, 1999.
[4] J. C. Nieto-Borge, G. Rodriguez, K. Hessner, and P. Izquierdo, "Inversion of marine radar images for surface wave analysis," *J. Atmos. Ocean. Technol.*, vol. 21, no. 8, pp. 1291–1300, 2004.
[5] H. Dankert, J. Horstmann, S. Lehner, and W. Rosenthal, "Detection of wave groups in SAR images and radar image sequences," *IEEE Trans. Geosci. Remote Sens.*, vol. 41, no. 6, pp. 1437–1446, Jun. 2003.
[6] C. Senet, J. Seemann, and F. Ziemer, "The near-surface current velocity determined from 5 image sequences of the sea surface," *IEEE Trans. Geosci. Remote Sens.*, vol. 39, no. 3, pp. 492–505, Mar. 2001.
[7] W. Huang, R. Carrasco, S. Chengxi, E. W. Gill, and J. Horstmann, "Surface current measurements using X-band marine radar with vertical polarization," *IEEE Trans. Geosci. Remote Sens.*, vol. 54, no. 5, pp. 2988–2997, May 2016.
[8] P. S. Bell and J. C. Osler, "Mapping bathymetry using X-band marine radar data recorded from a moving vessel," *Ocean Dyn.*, vol. 61, no. 12, pp. 2141–2156, 2011.
[9] J. J. Horstmann, R. Vicen-Bueno, and M. Coffin, "Reading the ocean with marine radars," in *Proc. Defence Global*, 2011, pp. 58–60.
[10] H. Dankert and J. Horstmann, "A marine radar wind sensor," *J. Atmos. Ocean. Technol.*, vol. 24, pp. 1629–1642, Sep. 2007.
[11] S. Salcedo-Sanz, J. C. Nieto Borge, L. Carro-Calvo, L. Cuadra, K. Hessner, and E. Alexandre, "Significant wave height estimation using SVR algorithms and shadowing information from simulated and real measured X-band radar images of the sea surface," *Ocean Eng.*, vol. 101, pp. 244–253, Apr. 2015.
[12] P. A. Hwang, M. A. Sletten, and J. V. Toporkov, "A note on Doppler processing of coherent radar backscatter from the water surface: With application to ocean surface wave measurements," *J. Geophys. Res.*, vol. 115, no. C3, p. C03026, 2010, doi: 10.1029/2009JC005870.
[13] R. Carrasco *et al.*, "A simple method for retrieving significant wave height from Dopplerized X-band radar," *Ocean Sci. Discussion*, vol. 13, no. 1, pp. 95–103, 2017.
[14] J. W. Plant and G. Farquharson, "Wave shadowing and modulation of microwave backscatter from the ocean," *J. Geophys. Res.*, vol. 117, no. C8, p. C08010, 2012, doi: 10.1029/2012JC007912.
[15] J. T. Johnson, R. J. Burkholder, J. V. Toporkov, D. R. Lyzenga, and W. J. Plant, "A numerical study of the retrieval of sea surface height profiles from low grazing angle radar data," *IEEE Trans. Geosci. Remote Sens.*, vol. 47, no. 6, pp. 1641–1650, Jun. 2009.
[16] N. Braun, F. Ziemer, A. Bezuglov, and M. Cysewski, "Sea-surface current features observed by Doppler-radar," *IEEE Trans. Geosci. Remote Sens.*, vol. 46, no. 4, pp. 1125–1133, Apr. 2008.
[17] P. H. Y. Lee *et al.*, "X band microwave backscattering from ocean waves," *J. Geophys. Res.*, vol. 100, no. C2, pp. 2591–2611, 1996.
[18] D. Miret, G. Soriano, F. Nouguier, P. Forget, M. Saillard, and C.-A. Guérin, "Sea surface microwave scattering at extreme grazing angle: Numerical investigation of the doppler shift," *IEEE Trans. Geosci. Remote Sens.*, vol. 52, no. 11, pp. 7120–7129, Nov. 2014.
[19] S. E. Belcher and J. C. R. Hunt, "Turbulent flow over hills and waves," *Annu. Rev. Fluid Mech.*, vol. 30, pp. 507–538, Sep. 1998.
[20] M. P. Buckley and F. Veron, "Structure of the airflow above surface waves," *J. Phys. Oceanogr.*, vol. 46, pp. 1377–1397, Sep. 2016.
[21] H. E. Krogstad, R. L. Gordon, and M. C. Miller, "High-resolution directional wave spectra from horizontally mounted acoustic Doppler current meters," *J. Atmos. Ocean. Technol.*, vol. 5, no. 2, pp. 340–352, 1988.
[22] T. H. C. Herbers, R. L. Lowe, and R. T. Guza, "Field verification of acoustic Doppler surface gravity wave measurements," *J. Geophys. Res.*, vol. 96, no. C9, pp. 17023–17035, 1991.
[23] M. A. de Schipper, R. C. de Zeeuw, S. de Vries, M. J. F. Stive, and J. Terwindt, "Horizontal ADCP measurements of waves and currents in the very nearshore," in *Proc. 10th Conf. Current, Waves Turbulence Meas.*, vol. 5759545. 2011, pp. 159–166, doi: 10.1109/CWTM.2011.5759545.
[24] G. S. Brown, "Guest editorial—Special issue on low-grazing-angle backscatter from rough surfaces," *IEEE Trans. Antennas Propag.*, vol. 46, no. 1, pp. 1–2, Jan. 1998.
[25] D. S. Zrnić, "Estimation of spectral moments for weather echoes," *IEEE Trans. Geosci. Electron.*, vol. 17, no. 4, pp. 113–128, Apr. 1979.
[26] L. Cornejo-Bueno, J. C. N. Borge, E. Alexandre, K. Hessner, and S. Salcedo-Sanz, "Accurate estimation of significant wave height with support vector regression algorithms and marine radar images," *Coastal Eng.*, vol. 114, pp. 233–243, Sep. 2016.

Ruben Carrasco received the B.Eng. degree in industrial engineering from the Universidad de Alcalá, Madrid, Spain, in 2009.

He was with the Department of Signal Theory and Communications, Universidad de Alcalá, working on his B.Eng. thesis related to ship detection in marine environments. From 2011 to 2014, he was a Remote Sensing Engineer with the Center for Maritime Research and Experimentation, NATO Science and Technology Organization, La Spezia, Italy. Since 2014, he has been a Research Engineer with the Department of Radar Hydrography, Institute of Coastal Research of the Helmholtz-Zentrum Geesthacht Centre for Materials and Coastal Research, Geesthacht, Germany. His research interests include artificial intelligence systems, radar signal processing, and pattern recognition.

Mr. Carrasco received in Arquimedes 2009 the Grupo Santander Award within Spain contest for young scientists.

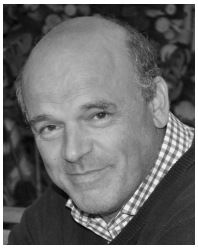

Jochen Horstmann received the Diploma (Dipl.-Oz.) degree in physical oceanography and the Ph.D. (Dr.rer.nat.) degree in earth sciences from the University of Hamburg, Hamburg, Germany, in 1997 and 2002, respectively.

In 1995, he joined the Helmholtz-Zentrum Geesthacht Centre for Materials and Coastal Research, Geesthacht, Germany. In 2002, he joined the Applied Physics Laboratory, John Hopkins University, Laurel, MD, USA, and the National Environmental Satellite, Data, and Information Service of NOAA, Washington, DC, USA, both as a Visiting Scientist. In 2004 and 2005, he was a Visiting Scientist with the Center for Southeastern Tropical Advanced Remote Sensing, University of Miami, FL, USA. From 2008 to 2013, he was a Senior Remote Sensing Scientist with the Center for Maritime Research and Experimentation, NATO Science and Technology Organization, La Spezia, Italy. Since 2002, he has been a Research Scientist with the Helmholtz-Zentrum Geesthacht Centre for Materials and Coastal Research. Since 2007, he has been an Adjunct Professor with the Rosenstiel School of Marine and Atmospheric Science, University of Miami. Since 2013, he has been the Head of the Department of Radar Hydrography, Institute of Coastal Research of the Helmholtz-Zentrum Geesthacht, Geesthacht. He has a wide experience in the field of radar remote sensing and has authored more than 55 articles in international peer-reviewed journals. His research interests include the development of oceanographic applications using radar-based sensors to investigate ocean-surface and near-surface processes.

Jörg Seemann received the Diploma degree in physics and the Ph.D. degree in geosciences from the University of Hamburg, Hamburg, Germany, in 1993 and 1997.

He has developed a method to retrieve high-resolution current and bathymetric maps from radar backscatter intensity images and is involved in the wave measurement with Doppler radar. He is currently a Research Scientist with the Radar Hydrography Department, Helmholtz-Zentrum Geesthacht Centre for Materials and Coastal Research, Geesthacht, Germany. His scientific focus is on oceanic and coastal radar remote sensing. His research interests include the development of signal and image processing algorithms to retrieve hydrographic parameters from incoherent and coherent radar data.